Line shape and frequency shift of Lamb dip and crossover-resonance dip in closely spaced transitions

Swapan Mandal and Pradip N. Ghosh*
Department of Physics, University of Calcutta, 92 Acharya Prafulla Chandra Road, Calcutta 700 009, India
(Received 12 March 1991; revised manuscript received 5 November 1991)

The line shape of a pair of Doppler-broadened closely spaced transitions sharing a common lower level and under the effect of a standing-wave monochromatic radiation field is studied. The eight steady-state optical Bloch equations are solved analytically to obtain the polarization by retaining terms up to the third power in the electric-field amplitude. The absorption coefficient derived for the standing-wave case consists of two Lamb dips for the two allowed transitions at ω_1 and ω_2 and a crossover resonance dip at the intermediate frequency $\omega_c=(\omega_1+\omega_2)/2$. The Lamp-dip peak frequencies show intensity-dependent shifts. Numerical computations are presented for different values of Rabi frequencies and relaxation linewidth parameters, which are small compared to the frequency difference $\Delta=\omega_2-\omega_1$. The computed line shape and frequency shift are compared with the observed results in the Balmer H_α line of hydrogen and the infrared Zeeman spectra of methane.

PACS number(s): 32.70.Jz, 33.70.Jg

I. INTRODUCTION

Nonlinear attenuation characteristics of Doppler-broadened atomic or molecular resonances involving closely spaced levels were studied in a number of theoretical [1–6] and experimental [7–10] work. Very narrow line widths of a variety of nonlinear-optical processes can be of great use for the determination of small splittings which may be inherently present in the atomic system (e.g., fine-structure or hyperfine splitting). Similar small splittings, induced in the atomic system by an external field (e.g., Zeeman effect), may also be resolved because of the narrow linewidth of the nonlinear resonances. In a standing wave, when the applied radiation field is sufficiently strong, the nonlinear resonance appears in the form of Lamb dip in the Doppler-broadened Gaussian background. The line shape of the Lamb-dip signal is Lorentzian and depends primarily on the natural linewidth and the collisional and saturation broadening. The increase of laser power increases the intensity of the signal at the cost of broadening it. In the case of closely spaced levels with the energy-level difference larger than the Rabi frequency and the collisional linewidth, but much smaller than the Doppler width, two distinct Lamb-dip signals appear when both the transitions are allowed. In the standing-wave arrangement, the nonresonant interactions with the oppositely moving waves lead to a crossover resonance which appears in the form of an additional dip at a frequency intermediate between the two resonance frequencies. Such additional resonances were predicted theoretically [1] and later observed experimentally in the laser saturation spectroscopy [7] of Balmer H_α line in hydrogen and also in the infrared Zeeman spectra of methane by laser-saturated absorption [8]. Hyperfine structure of methane was measured from the splitting of the closely spaced Lamb dips [9].

The line-shape theory of three-level systems under the effect of one or two incident electromagnetic radiations has been discussed in a number of theoretical work [1–6,11–17]. The line-shape theory for the two-level atoms, in the presence of two oppositely running electromagnetic waves of the same frequency and intensity, has been studied in detail [18–24]. Haroche and Hartmann [25] studied the saturated absorption line shape for the case of two-level atoms in the presence of a strong pump radiation and a counterrunning weak probe radiation of the same frequency. When an atomic system is irradiated by a strong electromagnetic wave, there can be modifications of atomic eigenstates leading to level shifts [26] or dynamic Stark splitting [27]. Haroche and Hartmann [25] showed that when one of the fields is very strong in a quasirunning-wave situation, there can be appreciable modification in the probe field transmission peak line shape. In a theoretical analysis of the saturation behavior of Doppler-broadened resonances involving closely spaced upper levels and a single lower level, Schlossberg and Javan [1] considered the effect of two closely spaced monochromatic electromagnetic fields having their frequencies within the Doppler width in a standing-wave arrangement. They investigated the effect of the third-order term in the electric-field amplitude on the absorption. The intensity of the crossover signal was shown to be given by the geometric mean of the two separate Lamb dips. Their calculations did not predict any shift of the two Lamb-dip frequencies. In the case of a single electromagnetic wave incident on the same system, we found by exact numerical solution of Bloch equations that the dips exhibit small shifts towards each other [6]. Any small intensity-dependent shift of the Lamb dips may account for important correction in the calculated hyperfine constants. A shift of the peak frequency of the Lamb dip from the atomic resonance frequency of the Balmer H_α line would lead to a correction to the Rydberg constant.

In this work, we present an analytical solution of the eight optical Bloch equations for the interaction of a

monochromatic standing wave with a three-level system having closely spaced upper levels. In our case the counterrunning waves have the same frequency and intensity. We shall consider the magnitude of field intensity to be such that the Rabi frequencies for both the transitions are small compared to the relaxational linewidth $(1/T)$. This enables a perturbation expansion of the absorption coefficient in terms of the electric-field amplitude ε. We shall retain terms up to the third power in ε. Our aim in this work is to investigate the effect of counterrunning waves on the line shape of closely spaced transitions. The computed line shape shows Lamb dips and a crossover resonance dip and predicts small intensity-dependent shift of peak frequencies. The calculated line shape of Balmer H_α line of hydrogen agrees with the observed spectrum. The computed line shapes are also compared with the infrared Zeeman spectra of methane.

II. THEORY

A. Optical Bloch equations

We consider an ensemble of nondegenerate three-level (a,b,c) quantum systems with $E_a<E_b<E_c$ and $E_c-E_b=\hbar\Delta$ is very small. A monochromatic radiation of electric-field amplitude ε and frequency ω is incident on the system. The frequency ω is close to the resonance frequencies $\omega_1=(E_b-E_a)/\hbar$ and $\omega_2=(E_c-E_a)/\hbar$, hence, $\Delta\omega_1=\omega-\omega_1$ and $\Delta\omega_2=\omega-\omega_2$ are very small. We first consider the three-level systems to have zero velocity and to have no interaction with each other. The dynamics of the system may be described by the Liouville equations for the 3×3 density matrix (Appendix A). The diagonal elements of the density matrix define the population difference

$$\Delta N_1=N(\rho_{aa}-\rho_{bb})$$

and (1)

$$\Delta N_2=N(\rho_{aa}-\rho_{cc}) ,$$

where N is the number of atoms per unit volume. The diagonal elements ρ_{aa}, ρ_{bb}, and ρ_{cc} are replaced by their volume averages [16] so that population pulsation effects do not appear. The real and imaginary parts of the polarizations P_1 and P_2 associated with the two dipole-allowed transitions $a\rightarrow b$ and $a\rightarrow c$, respectively, are (Appendix A)

$$P_{1r}+iP_{1i}=N\mu_{ba}\rho_{ab} , \tag{2}$$

and

$$P_{2r}+iP_{2i}=N\mu_{ca}\rho_{ac} . \tag{3}$$

The Rabi frequencies are defined as

$$x_1=2\mu_{ab}\varepsilon/\hbar$$

and (4)

$$x_2=2\mu_{ac}\varepsilon/\hbar .$$

The transition $b\rightarrow c$ is not allowed and there is no radiation corresponding to this energy difference, but the time development of ρ_{bc} is not zero [Eq. (A8) in Appendix A]. The time developments of P_1 and P_2 involve terms like $\mu_{ca}\mu_{ab}\rho_{bc}$. Such terms are defined as [6,14]

$$P_{nr}+iP_{ni}=N\mu_{ca}\mu_{ab}\rho_{bc} . \tag{5}$$

The polarizations P_1 and P_2 are modified to the order x_1x_2 through the coupling matrix element ρ_{bc}. Hence, the terms P_n produce higher-order correction to P_1 and P_2. The physical significance of these terms was discussed earlier [6].

The steady-state optical Bloch equations are (Appendix A)

$$P_{1r}/T_2-\Delta\omega_1P_{1i}-\varepsilon P_{ni}/\hbar=0 , \tag{6a}$$

$$P_{2r}/T_2-\Delta\omega_2P_{2i}+\varepsilon P_{ni}/\hbar=0 , \tag{6b}$$

$$\Delta N_1/T_1-4\varepsilon P_{1i}/\hbar-2\varepsilon P_{2i}/\hbar=\Delta N_{10}/T_1 , \tag{6c}$$

$$\Delta N_2/T_1-2\varepsilon P_{1i}/\hbar-4\varepsilon P_{2i}/\hbar=\Delta N_{20}/T_1 , \tag{6d}$$

$$P_{1i}/T_2+\Delta\omega_1P_{1r}-\varepsilon P_{nr}/\hbar+\varepsilon|\mu_{ab}|^2\Delta N_1/\hbar=0 , \tag{6e}$$

$$P_{2i}/T_2+\Delta\omega_2P_{2r}-\varepsilon P_{nr}/\hbar+\varepsilon|\mu_{ac}|^2\Delta N_2/\hbar=0 , \tag{6f}$$

$$P_{nr}/T_n+\Delta P_{ni}+\varepsilon|\mu_{ac}|^2P_{1i}/\hbar+\varepsilon|\mu_{ab}|^2P_{2i}/\hbar=0 , \tag{6g}$$

$$P_{ni}/T_n-\Delta P_{nr}-\varepsilon|\mu_{ab}|^2P_{2r}/\hbar+\varepsilon|\mu_{ac}|^2P_{1r}/\hbar=0 . \tag{6h}$$

The longitudinal (T_1) and transverse (T_2,T_n) relaxation times are introduced phenomenologically. When the field is withdrawn, the polarization terms relax to their equilibrium zero values while the population differences relax to the equilibrium values ΔN_{10} and ΔN_{20} determined by the Boltzmann distribution.

B. Doppler-broadened standing-wave absorption

Equations (6) are solved to obtain the polarization and population difference as

$$P_{1i}=-\frac{\hbar}{4\varepsilon}x_1^2L_1(\omega)[\Delta N_{10}-\tfrac{1}{2}L_2(\omega)A(\omega)x_2^2\Delta N_{20}] \tag{7}$$

and

$$\Delta N_1=\Delta N_{10}\{1-x_1^2T_1L_1(\omega)[1-\tfrac{1}{4}x_2^2L_2(\omega)]\}$$
$$-\tfrac{1}{2}\Delta N_{20}x_2^2T_1L_2(\omega)[1-x_1^2L_1(\omega)A(\omega)] , \tag{8}$$

where

$$L_1(\omega)=[1/T_2+\Delta\omega_1^2T_2+x_1^2T_1+\tfrac{1}{4}x_2^2T_n-\tfrac{1}{4}x_2^2(\Delta T_n+\Delta\omega_1T_2)^2/D]^{-1} , \tag{9}$$

$$A(\omega)=T_1+\tfrac{1}{2}T_n-(\Delta T_n+\Delta\omega_1T_2)(\Delta T_n-\Delta\omega_2T_2)/2D , \tag{10}$$

and

$$D=1/T_n+\Delta^2 T_n+(x_1^2+x_2^2)T_2/4 \ . \tag{11}$$

The expressions for P_{2i}, ΔN_2, and $L_2(\omega)$ are obtained from the equations (7)–(9), respectively, by interchanging the subscripts 1 and 2 in x_k, $L_k(\omega)$, $\Delta\omega_k$, and ΔN_{k0}. The expression for $L_1(\omega)$ in Eq. (9) may be simplified to the following form:

$$L_1(\omega)=\frac{4DT_2'}{T_2(4D-x_2^2T_2)}\frac{1/T_2'}{(\Delta\omega_1^s)^2+1/T_2'^2} \ , \tag{12}$$

where

$$\Delta\omega_1^s=\omega-\left[\omega_1+\frac{x_2^2\Delta}{4(\Delta^2+1/T_n^2)+x_1^2T_2/T_n}\right] \tag{13}$$

and

$$\frac{1}{T_z'}=\frac{1}{T_2}\frac{DT_n[1+T_1T_2x_1^2(1+\Delta^2T_n^2)/DT_n]^{1/2}}{1+\Delta^2T_n^2+x_1^2T_nT_2/4} \ . \tag{14}$$

Similarly, we obtain

$$L_2(\omega)=\frac{4DT_2''}{T_2(4D-x_1^2T_2)}\frac{1/T_2''}{(\Delta\omega_2^s)^2+1/T_2''^2} \ , \tag{15}$$

where

$$\Delta\omega_2^s=\omega-\left[\omega_2-\frac{x_1^2\Delta}{4(\Delta^2+1/T_n^2)+x_2^2T_2/T_n}\right] , \tag{16}$$

and T_2'' may be obtained from T_2' in Eq. (14) by interchanging x_1 and x_2.

In order to include the Doppler shift in a standing-wave case, we have to replace $\Delta\omega_1$ and $\Delta\omega_2$ by $\Delta\omega_1\pm\omega'$ and $\Delta\omega_2\pm\omega'$, where $\omega'=\omega v/c$, v is the molecular velocity and c is the velocity of light. When the atomic system is enclosed in a cavity, there are two waves moving in opposite directions and interacting with the molecules with velocity v. The imaginary part of the total polarization in this case would be

$$P_i=P_{1i+}+P_{1i-}+P_{2i+}+P_{2i-} \ , \tag{17}$$

where $P_{1i\pm}$ mean the polarization due to the transition $a\rightarrow b$ induced by the waves moving in opposite directions. Similarly, $P_{2i\pm}$ stand for the same due to the transition $a\rightarrow c$. In order to calculate $P_{1i\pm}$ from Eq. (7), one has to consider the fact that, in the presence of a standing wave, ΔN_1 relaxes to $\Delta N_{1\mp}$ when the field $2\varepsilon\cos(\omega t\pm kz)$ is withdrawn and not to ΔN_{10} as in the case of a traveling wave. Similarly, for $P_{2i\pm}$, ΔN_2 relaxes to $\Delta N_{2\mp}$ with the withdrawal of the field. The expressions for $\Delta N_{1\pm}$ are obtained from ΔN_1 in Eq. (8) by replacing $\Delta\omega_1$ with $\Delta\omega_1\pm\omega'$.

The polarization P_i induced by the electric field on the three-level atomic system is calculated from Eq. (17) after using Eqs. (7)–(16) and is obtained in the form

$$P_i=P_i^{(1)}+P_i^{(3)}+P_i^{(5)}+\cdots \ , \tag{18}$$

where the term $P_i^{(n)}$ depends linearly on ε^n. This result may also be obtained from time-dependent perturbation theory when one solves the Liouville equations (Appendix A) for the density matrix. The density matrix can be written as a perturbation series in terms of the interaction Hamiltonian. Such an approximation of the density matrix would lead to the series expansion [Eq. (18)] for polarization [28].

For a small field, the series in Eq. (18) converges rapidly. We shall retain terms up to the third power [29] in ε. The effects of the next higher-order term are given in Appendix B. By omitting all the terms with powers of ε higher than three we obtain

$$\begin{aligned}P_i=-\frac{\hbar x_1^2}{4\varepsilon}\{&\Delta N_{10}[L_{1+}(\omega)+L_{1-}(\omega)-2x_1^2T_1L_{1+}(\omega)L_{1-}(\omega)]\\&-\tfrac{1}{2}\Delta N_{20}x_2^2[T_1L_{1-}(\omega)L_{2+}(\omega)+T_1L_{1+}(\omega)L_{2-}(\omega)+L_{1-}(\omega)L_{2-}(\omega)A_-(\omega)\\&+L_{1+}(\omega)L_{2+}(\omega)A_+(\omega)]\}+(1\rightleftarrows 2) \ ,\end{aligned} \tag{19}$$

where the subscripts $\pm$ correspond to $\pm$ signs in front of ω' and the last term is obtained by interchanging the subscripts 1 and 2 in x_k, ΔN_{k0}, and $L_{k\pm}(\omega)$ and of $\Delta\omega_k$ in $A_\pm(\omega)$ in the first term. Assuming a Maxwell velocity distribution law, we can obtain the total absorption coefficient

$$\gamma(\omega)=\frac{4\sqrt{\pi}\omega q}{c\varepsilon}\int P_i(\omega')\exp(-q^2\omega'^2)d\omega' \ , \tag{20}$$

where

$$q=\frac{c}{\omega}(M/2kT_B)^{1/2} \tag{21}$$

is the Doppler-broadening parameter where T_B is the Boltzmann temperature and M is the molecular mass. In the Doppler-broadened limit of large T_2, we can approximate

$$\frac{1/T_2}{(\Delta\omega\pm\omega')^2+1/T_2^2}=\pi\delta(\Delta\omega\pm\omega') \ . \tag{22}$$

C. Line shape and frequency shift

Substituting Eqs. (8), (10), (12), (15), and (19) in Eq. (20) and using the approximation of Eq. (22), we obtain, after the velocity integration,

$$\gamma(\omega)=\frac{8\pi^{3/2}q\omega}{c\hbar}|\mu_{ab}|^2\exp[-(q\Delta\omega_1^s)^2]$$
$$\times\left\{\Delta N_{10}-\Delta N_{10}x_1^2T_1\frac{1/T_2'}{4(\Delta\omega_1^s)^2+(1/T_2')^2}\right.$$
$$-\tfrac{1}{4}(\Delta N_{10}+\Delta N_{20})x_2^2\left[\frac{T_1/T_2''}{(\Delta\omega_1^s+\Delta\omega_2^s)^2+(1/T_2'')^2}\right.$$
$$\left.\left.+\left[T_1+T_n/2+\frac{\Delta^2(T_n-T_2)}{2(\Delta^2+1/T_n^2)}\right]\frac{1/T_2''}{(\Delta\omega_1^s-\Delta\omega_2^s)^2+(1/T_2'')^2}\right]\right\}+(1\rightleftarrows 2)\ . \tag{23}$$

The last term is obtained from the first one by replacing μ_{ab} by μ_{ac} and interchanging the subscripts 1 and 2 in x_k, ΔN_{k0}, and $\Delta\omega_k^s$. Equation (23) expresses the Doppler-broadened absorption line shape together with Lamb dips having Lorentzian line shape. In order to observe two resolved Lamb dips, Δ should be larger than the Rabi frequency and the inverse of relaxation time. It is interesting to note that the peak frequencies are shifted in such a way that they approach each other. The shift [Eqs. (13) and (16)] is proportional to the laser intensity when the Rabi frequency is smaller compared to Δ and $1/T_n$. It also depends on Δ in such a way that, for Δ much large compared to x_1 and $1/T_n$ it is inversely proportional to Δ. If Δ is smaller than x and $1/T_n$, the shift is proportional to Δ, but in this case Lamb dips are not resolved. The intensity dependence of the shift may be compared with the dynamic Stark effect or Autler-Townes effect [27]. The shift in the present case arises from the nonresonant interaction between the closely spaced levels and it vanishes for large Δ. A similar shift of the Doppler free absorption peak frequencies was also obtained by us from the numerical solution of the Bloch equations [6]. The shift disappears when the terms P_n involving the product of μ_{ab} and μ_{ac} are omitted.

D. Crossover resonance

In addition to the Lamb dips at $\Delta\omega_1^s=0$ and $\Delta\omega_2^s=0$, Eq. (23) predicts an additional dip when $\Delta\omega_1^s+\Delta\omega_2^s=0$, i.e, at a frequency

$$\omega=(\omega_1+\omega_2)/2+\frac{\Delta T_n}{2}\left[\frac{x_2^2}{4D-x_2^2T_2}-\frac{x_1^2}{4D-x_1^2T_2}\right]. \tag{24}$$

When $x_1=x_2$, the dip occurs at the intermediate frequency $\omega_c=(\omega_1+\omega_2)/2$. This dip is known as the crossover resonance dip [1,24]. In this case the left-traveling component at ω is Doppler shifted to ω_2 (or ω_1) for atoms of an appropriate velocity, while for the atoms with the same velocity the right-traveling component at ω is Doppler shifted to ω_1 (or ω_2). When x_1 is not equal to x_2, the crossover resonance will shift towards the stronger Lamb dip. The last term in Eq. (23) is independent of frequency and depends on $\Delta=\omega_2-\omega_1$ only. This term becomes important in the energy-level-tuned level-crossing experiments.

III. COMPUTATION OF LINE SHAPE AND SHIFT

We have computed the line shape [Eq. (23)] for different values of Δ, x_1, x_2, and $T_1=T_2=T_n=T$, which are assumed to be equal. The parameters used for computation are chosen, as far as possible, to correspond to the observed [7,30,31] Balmer H_α transitions $2S_{1/2}$-$3P_{1/2}$ and $2S_{1/2}$-$3P_{3/2}$ sharing the common level $2S_{1/2}$ and corresponding to the frequency region 15 230 cm^{-1}. The Doppler broadening in this region is very large. For these closely spaced transitions, $\Delta=3.3$ GHz and the parameters x ($=x_1=x_2$) and T's are so chosen that the approximate linewidth $(x^2+1/T^2)^{1/2}$ is much less than Δ. The observed linewidth is of the order of 0.7 GHz. The

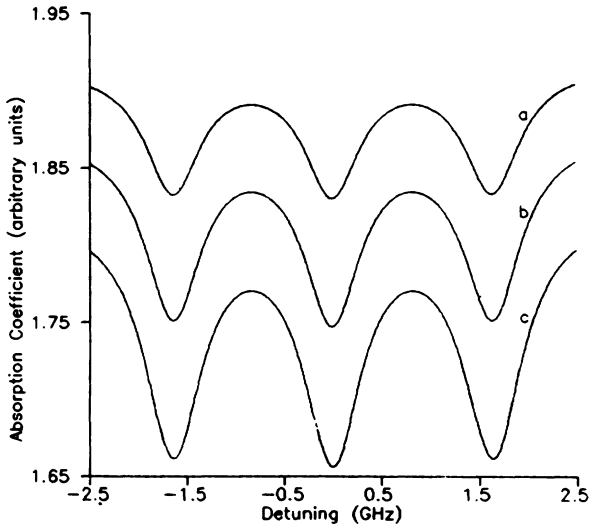

FIG. 1. Absorption line shape in the visible region for various Rabi frequencies (*a*) $x=0.2$ GHz, (*b*) $x=0.25$ GHz, and (*c*) $x=0.3$ GHz with fixed relaxation time $T=1.5$ nsec and $\Delta=3.3$ GHz. The detuning corresponds to $\omega-\omega_c$.

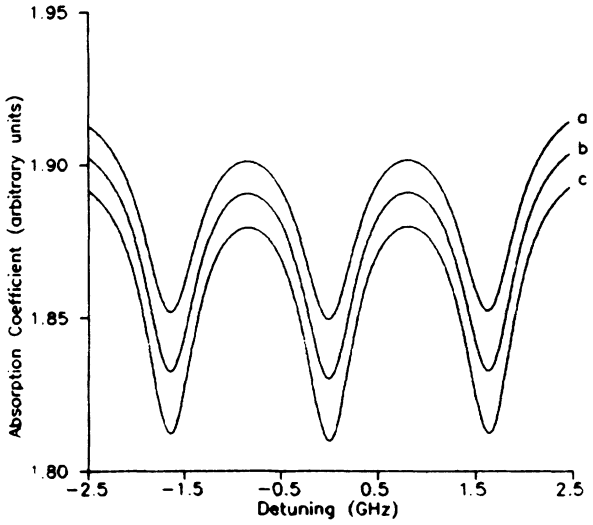

FIG. 2. Absorption line shape in the visible region for various relaxation times (*a*) $T=1.4$ nsec. (*b*) $T=1.5$ nsec, and (*c*) $T=1.6$ nsec with fixed Rabi frequency $x=0.2$ GHz and $\Delta=3.3$ GHz. The detuning corresponds to $\omega-\omega_c$.

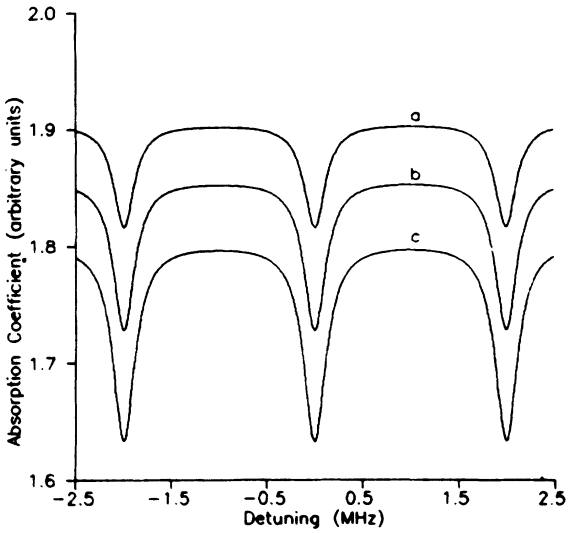

FIG. 4. Absorption line shape in the ir region for various Rabi frequencies (*a*) $x=0.08$ MHz, (*b*) $x=0.1$ MHz, and (*c*) $x=0.12$ MHz with fixed relaxation time $T=4.0$ μsec and $\Delta=4.0$ MHz. The detuning corresponds to $\omega-\omega_c$.

computed line shapes for $T=1.5$ nsec and the values of x in the range 0.2–0.3 GHz are shown in Fig. 1. It is interesting to note that the peak height of the crossover Lamb dip is very close to those of the Lamb dips. This arises from the fact that the intensity of the crossover Lamb dip is given by the geometric mean [1] of the Lamb dips at ω_1 and ω_2. An interesting feature of the computed line shape is the shift of the Lamb dips ω_1 and ω_2 towards each other, as predicted by Eqs. (13) and (16). Since $x_1=x_2$, the crossover Lamb dip does not exhibit any shift. The curves (Fig. 1) show rapid increase in the Lamb-dip intensity with Rabi frequency. Similarly, the curves in Fig. 2 show the sharpening of Lamb dips with increase of relaxation time T. We have computed the shift of ω_1 with laser power in the range 2–250 mW/mm^2 as used in Ref. [7]. Using a computed value of the oscillator strength for the $2S$-$3P$ transition of hydrogen, we obtain the values of x in the range 0.01–0.15 GHz, which are proportional to the square root of the laser intensity. Hence, the shift of $\Delta\omega_1$ given by Eq. (13) varies linearly with the laser intensity. From the computed curve (Fig. 3) we obtain a shift of 12 [kHz/(mW/mm^2)] or 1 part in 4×10^{10} per mW/mm^2 of the laser power. This is within the experimental upper limit [7] of the intensity-dependent shift of 2 parts in 10^{10} per mW/mm^2.

We have further computed the line shape of the Lamb dips in the infrared region which were observed in methane [8]. The curves show the effects of variable Rabi frequency with constant relaxation time (Fig. 4) and of variable relaxation time with constant Rabi frequency

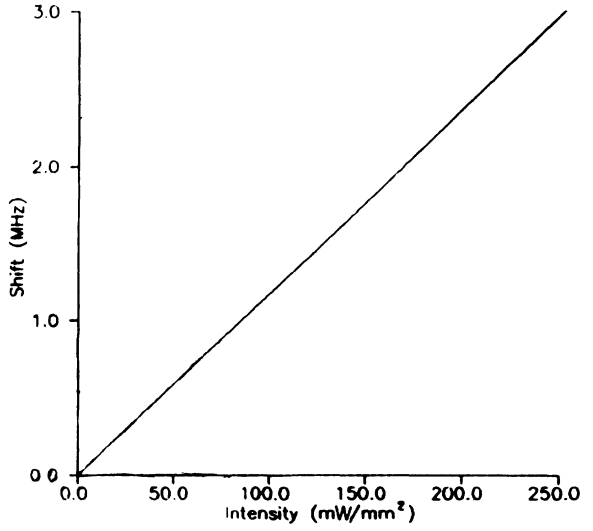

FIG. 3. Shift in the Lamb-dip position vs field intensity with $T=5.0$ nsec and $\Delta=3.3$ GHz (see text).

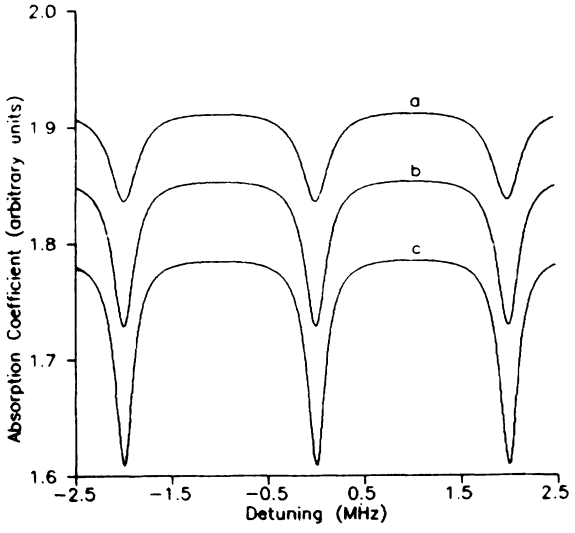

FIG. 5. Absorption line shape in the ir region for various relaxation times (*a*) $T=3.0$ μsec, (*b*) $T=4.0$ μsec, and (*c*) $T=5.0$ μsec with fixed Rabi frequency $x=0.1$ MHz and $\Delta=4.0$ MHz. The detuning corresponds to $\omega-\omega_c$.

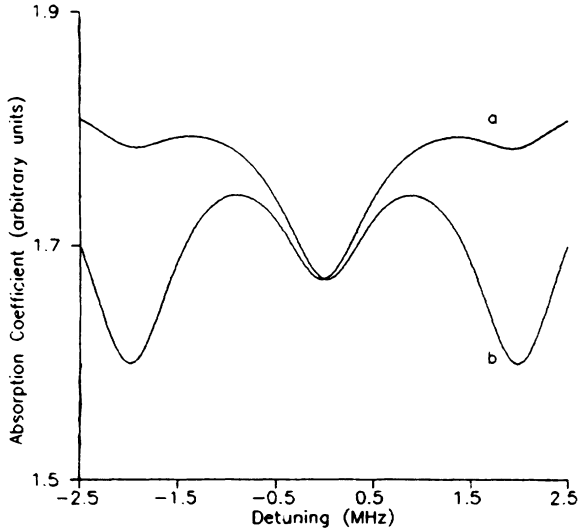

FIG. 6. Absorption line shape in the ir region for (*a*) $x_1=0.6$ and $x_2=0.2$ MHz, (*b*) $x_1=0.2$ and $x_2=0.6$ MHz with $T=1.0$ μsec and $\Delta=4.0$ MHz. The detuning corresponds to $\omega-\omega_c$.

(Fig. 5). In this case, the crossover Lamb dip also has the same intensity as the Lamb dips. Figure 6 shows the shift of crossover Lamb dip when $x_1\neq x_2$. It should be noted that the shifts of the Lamb dips lead to a decrease of Δ by 8 kHz at $x=0.25$ MHz and $T=3.0$ μsec (Fig. 7). Since the value of Δ is useful in the calculation of g factor or hyperfine splitting constants, such intensity-dependent shifts may be important in the calculation of these parameters. For an estimation of the correction due to the shift of peak frequency, one must have an accurate knowledge of T and the laser intensity.

It is to be noted that the observed infrared Zeeman spectra of methane by Uzgiris *et al.* [8] show that the intensity of the crossover Lamb dip is much smaller compared to the lamb dips of the parent transitions, although our theoretical computation predicts the crossover Lamb dip to have the same intensity as the other dips. Our result is in agreement with that of Schlossberg and Javan [1]. It may be mentioned here that Cardimona *et al.* [32] deduced the effect of quantum electrodynamic corrections [33] on the steady-state absorption line shape of a single traveling wave. They showed that when the dipole moments μ_{ab} and μ_{ac} are parallel and equal in magnitude, then the total absorption rate vanishes at the intermediate frequency ω_c. In absence of the quantum electrodynamic effect, a nonzero absorption is found at ω_c for a single running wave [6]. Hence, the inclusion of the additional damping terms arising from the quantum electrodynamic effect would lead to similar vanishing of the absorption at ω_c if the dipole moments are properly matched. The crossover Lamb dip which arises from the nonlinear resonance of the oppositely running waves would be superimposed on this. Thus, the quantum electrodynamic effect will lead to a decrease of the observed intensity at ω_c. However, such a decrease is possible only if the transition moments obey the above condition.

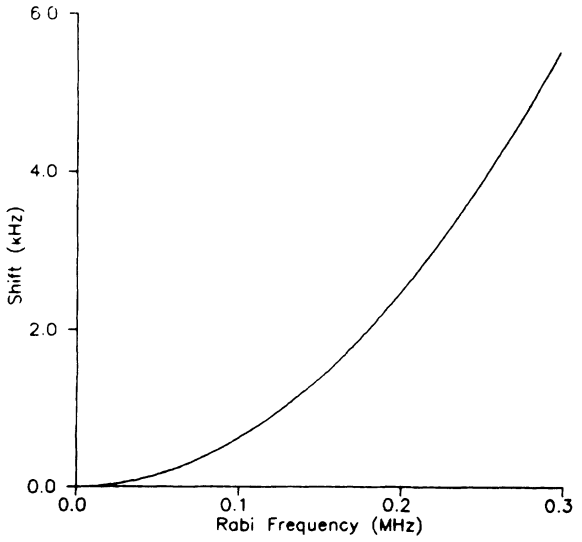

FIG. 7. Shift of the Lamb-dip position vs Rabi frequency with $T=3.0$ μsec and $\Delta=4.0$ MHz (see text).

IV. DISCUSSIONS AND CONCLUSIONS

In this work, the Doppler-broadened absorption line shape for coupled closely spaced transitions in the presence of a standing wave has been presented. The Bloch equations are solved to obtain the polarization by retaining terms up to the third power in the electric field. Hence, the shift is obtained in the fifth power of interaction. The fifth power terms in electric-field amplitude ε in the line shape lead to a correction to the frequency shift in the seventh order of interaction. The correction in the line shape arising from these terms is given in Appendix B. But numerical computation shows that it has negligible effect on the line shape and frequency shift for the values of Rabi frequencies used in our work.

The computed line shape predicts intensity-dependent shifts of the Lamb-dip frequencies. In the present case, the shifts are such that the dips approach each other so that the splitting is reduced. The computed intensity dependence of the shift of Lamb dip is within the estimated intensity-dependent shift of the observed Balmer H_α line of hydrogen [7]. The observed intensity-dependent shift may also arise partly from the dynamic Stark effect [27] or Bloch-Siegert effect [34]. Similar shifts in the infrared region may also be responsible for small correction of the observed hyperfine [9] and Zeeman splitting [8] which may lead to small corrections of the computed hyperfine interaction constant or the g factor of the molecule.

It may be noted that in our work we have used a standing wave with the same field strength for the copropagating and counterpropagating waves. The field strength is taken to be such that a perturbation-type calculation is allowed and the small third-order term leads to Lamb dips in the large Gaussian background. If one of the waves is very strong and acts as a pump, while the other wave is weak, one has to use a semiperturbative technique, as used in Ref. [25], to obtain the line shape in a two-level atomic system. The additional features computed by Haroche and Hartmann [25] would also be expected in the three-level system. But these features are

very small in intensity. In the experimental work [7,30,31] on Balmer H_α lines involving closely spaced upper levels, a strong pump and a weak probe were used, but no additional resonances, predicted theoretically [25], were reported. Haroche and Hartmann [25] obtained a small light shift of the resonance peak at $\omega=\omega_0$, where ω_0 is the resonance frequency of the two-level system. The light shift arose from the strong pump. The shift obtained by us is also intensity dependent but it arises from the closely spaced levels. It disappears when Δ is very large. It must be mentioned that our calculations are not attempted to obtain a fitting of the spectral lines. Hence, we have used the same values for the relaxation times.

We have presented the line shape for transitions in the visible and infrared region for different values of relaxation time T and Rabi frequencies. These curves may be useful for comparison with the actual observed curves. The peak height of the crossover resonance is in agreement with the observed spectra of the Balmer H_α line of hydrogen [7]. But the observed intensity of the crossover resonance in the infrared Zeeman spectra [8] of methane is much smaller than our computed result. Such a discrepancy may arise from the quantum electrodynamic correction terms [32] which depend on the relative orientation and magnitude of the transition dipole moments of the coupled transitions. Such corrections may be useful when the two dipoles are parallel and equal in magnitude.

In this work we have investigated the line shape of the frequency-tuned absorption. Hence, the last term in Eq. (23) is constant for our case. In the case of energy-level-tuned spectroscopy this term would lead to Zeeman coherence effect [35] analogous to the Hanle resonance.

ACKNOWLEDGMENTS

One of the authors (S.M.) thanks the University Grants Commission, New Delhi for support. The authors also thank the University Grants Commission for the facilities made available to them through a Departmental Special Assistance Programme.

APPENDIX A

The Hamiltonian of the atomic system interacting with the electromagnetic field is

$$H=H_0-\mu[\varepsilon\exp(i\omega t-ikz)+\text{c.c.}]\ , \tag{A1}$$

where μ is the dipole moment operator, H_0 is the unperturbed Hamiltonian of the three-level system with the eigenvalues E_a, E_b, E_c, and $k=\omega/c$ for a plane wave in vacuum. The density matrix corresponding to the Hamiltonian of Eq. (A1) satisfies the equation

$$i\hbar\frac{\partial\sigma}{\partial t}=[H,\sigma]\ . \tag{A2}$$

Following Refs. [11,14], the rate equations for the components of the density matrix ρ in the interaction representation and under the rotating-wave approximation are

$$i\hbar\frac{\partial}{\partial t}\rho_{aa}=\varepsilon(\rho_{ab}\mu_{ba}+\rho_{ac}\mu_{ca})-\varepsilon(\mu_{ab}\rho_{ba}+\mu_{ac}\rho_{ca})\ , \tag{A3}$$

$$i\hbar\frac{\partial}{\partial t}\rho_{bb}=\varepsilon(\rho_{ba}\mu_{ab}-\mu_{ba}\rho_{ab})\ , \tag{A4}$$

$$i\hbar\frac{\partial}{\partial t}\rho_{cc}=\varepsilon(\rho_{ca}\mu_{ac}-\mu_{ca}\rho_{ac})\ , \tag{A5}$$

$$i\hbar\frac{\partial}{\partial t}\rho_{ab}=\varepsilon\mu_{ab}(\rho_{aa}-\rho_{bb})-\varepsilon\mu_{ac}\rho_{cb}+\hbar\Delta\omega_1\rho_{ab}\ , \tag{A6}$$

$$i\hbar\frac{\partial}{\partial t}\rho_{ac}=\varepsilon\mu_{ac}(\rho_{aa}-\rho_{cc})-\varepsilon\mu_{ab}\rho_{bc}+\hbar\Delta\omega_2\rho_{ac}\ , \tag{A7}$$

$$i\hbar\frac{\partial}{\partial t}\rho_{bc}=\varepsilon\rho_{ba}\mu_{ac}-\varepsilon\mu_{ba}\rho_{ac}-\hbar\Delta\rho_{bc}\ , \tag{A8}$$

under the effect of the applied field a macroscopic polarization will develop, which can be written as

$$P=N[\mu_{ba}\rho_{ab}+\mu_{ca}\rho_{ac}]\exp[i(\omega t-kz)]+\text{c.c.}\ , \tag{A9}$$

which leads to the definition of the real and imaginary parts of polarizations given in Eqs. (2) and (3).

Time derivatives of Eqs. (1)–(3) and (5) together with Eqs. (A2)–(A8) lead to the optical Boch equations (6) when the phenomenological relaxations are added.

APPENDIX B

The fifth-order term in Eq. (18) for polarization is obtained as

$$\begin{aligned}P_i^{(5)}=\frac{\hbar}{8\varepsilon}x_1^2x_2^2T_1(&\Delta N_{10}x_1^2L_{1+}(\omega)L_{1-}(\omega)[L_{2+}(\omega)A_+(\omega)+L_{2-}(\omega)A_-(\omega)]\\&+\Delta N_{20}\{x_1^2L_{1+}(\omega)L_{1-}(\omega)[L_{2+}(\omega)A_+(\omega)+L_{2-}(\omega)A_-(\omega)]\\&+x_2^2L_{2+}(\omega)L_{2-}(\omega)[L_{1+}(\omega)A_+(\omega)+L_{1-}(\omega)A_-(\omega)]\}\ )+(1\rightleftarrows2)\ .\end{aligned} \tag{B1}$$

Using the procedure outlined in Eqs. (20)–(23), we obtain, for the contribution to the absorption coefficient due to the fifth-order terms in polarizations [Eq. (B1)],

$$\begin{aligned}\gamma'(\omega)=&\frac{8\pi^{3/2}q\omega}{c\hbar}|\mu_{ab}|^2\exp[-(q\Delta\omega_1^s)^2]\\&\times\left[\frac{1}{8}\Delta N_{10}x_1^2x_2^2T_nT_2^2\frac{1}{1+\Delta^2T_n^2}(T_1-T_n/4)+\Delta N_{10}x_1^4T_1^2T_2\frac{1/T_2'}{4(\Delta\omega_1^s)^2+(1/T_2')^2}\right.\\&+\frac{1}{4}T_1x_2^2(\Delta N_{10}+\Delta N_{20})\left[T_1+T_n/2-\frac{\Delta^2T_n^2(T_n+T_2)}{2(1+\Delta^2T_n^2)}\right]\\&\left.\times\left[x_1^2\frac{1/T_2'}{4(\Delta\omega_1^s)^2+1/T_2'^2}+x_2^2\frac{1/T_2''}{(\Delta\omega_1^s+\Delta\omega_2^s)^2+(1/T_2'')^2}\right]\frac{1/T_2''}{(\Delta\omega_1^s-\Delta\omega_2^s)^2+(1/T_2'')^2}\right]+(1\rightleftarrows2)\ .\end{aligned} \tag{B2}$$

*Corresponding author.

[1] H. R. Schlossberg and A. Javan, Phys. Rev. **150**, 267 (1966).
[2] M. S. Feld and A. Javan, Phys. Rev. **177**, 540 (1969).
[3] W. R. Bennet, Jr. and P. J. Kindlman, Phys. Rev. **149**, 38 (1966).
[4] S. Stenholm, Phys. Rep. C **6**, 1 (1973).
[5] C. Feuillade and C. Bottcher, Chem. Phys. **62**, 67 (1981).
[6] P. N. Ghosh and S. Mandal, Chem. Phys. Lett. **164**, 279 (1989).
[7] T. W. Hänsch, M. H. Nayfeh, S. A. Lee, S. M. Curry, and I. S. Shahin, Phys. Rev. Lett. **32**, 1336 (1974).
[8] E. E. Uzgiris, J. L. Hall, and R. L. Barger, Phys. Rev. Lett. **26**, 289 (1971).
[9] J. L. Hall and C. Borde, Phys. Rev. Lett. **30**, 1101 (1973).
[10] V. S. Letokhov and V. P. Chebotayev, *Nonlinear Laser Spectroscopy* (Springer-Verlag, Berlin, 1977).
[11] J. C. McGurk, T. G. Schmalz, and W. H. Flygare, Adv. Chem. Phys. **25**, 1 (1974).
[12] V. P. Chebotayev, in *High Resolution Laser Spectroscopy,* edited by K. Shimoda (Springer-Verlag, Berlin, 1976), p. 201.
[13] M. Takami, Jpn. J. Appl. Phys. **15**, 1063 (1976).
[14] S. Ghoshal and P. N. Ghosh, J. Chem. Phys. **83**, 4015 (1985).
[15] C. Feuillade and P. Berman, Phys. Rev. A **29**, 1236 (1984).
[16] S. Stenholm, *Foundations of Laser Spectroscopy* (Wiley, New York, 1983).
[17] S. Ghoshal and P. N. Ghosh, Opt. Commun. **73**, 455 (1989).
[18] W. E. Lamb, Jr., Phys. Rev. **134**, 1429 (1964).
[19] S. Stenholm and W. E. Lamb, Jr., Phys. Rev. **181**, 618 (1969).
[20] B. J. Feldman and M. S. Feld, Phys. Rev. A **1**, 1375 (1970).
[21] H. K. Holt, Phys. Rev. A **2**, 233 (1970).
[22] T. W. Hänsch and P. Toschek, Z. Phys. **236**, 213 (1970).
[23] E. V. Baklanov and V. P. Chebotayev, Zh. Eksp. Teor. Fiz. **60**, 552 (1971) [Sov. Phys. JETP **33**, 300 (1971)].
[24] M. D. Levenson and S. S. Kano, *Introduction to Nonlinear Laser Spectroscopy* (Academic, New York, 1988), Chap. 3.
[25] S. Haroche and F. Hartmann, Phys. Rev. A **6**, 1280 (1972).
[26] C. Cohen-Tannoudjii and J. Dupont-roe, Phys. Rev. A **5**, 968 (1972).
[27] S. H. Autler and C. H. Townes, Phys. Rev. **100**, 703 (1955).
[28] M. Weissbluth, *Photon Atom Interactions* (Academic, New York, 1989).
[29] M. Sargent III, M. O. Scully, and W. E. Lamb, Jr., *Laser Physics* (Addison-Wesley, London, 1974).
[30] T. W. Hänsch, A. L. Schawlow, and G. W. Series, Sci. Am. **240**, 72 (1979).
[31] W. Demtröder, *Laser Spectroscopy* (Springer, Berlin, 1982), p. 249.
[32] D. A. Cardimona, M. G. Raymer, and C. R. Stroud, Jr., J. Phys. B **15**, 55 (1982).
[33] P. W. Milonni, Phys. Rep. C **25**, 1 (1976).
[34] L. Allen and J. H. Eberly, *Optical Resonance and Two-Level Atoms* (Wiley, New York, 1975).
[35] B. Stahlberg, M. Lindberg, and P. Jungner, J. Phys. B **18**, 627 (1985).